# Multiscale modeling of surface sputtering in a scanning transmission electron microscope

W. S. Lai,* A. V. Barashev, and D. J. Bacon
*Materials Science and Engineering, Department of Engineering, The University of Liverpool, Brownlow Hill, Liverpool L69 3GH, United Kingdom*

(Received 24 January 2004; revised manuscript received 22 July 2004; published 22 November 2004)

A model to describe modification of surface shape and chemical composition of a specimen due to sputtering in a scanning transmission electron microscope is presented. It employs Monte Carlo simulation of electron trajectories, molecular dynamics modeling of individual sputtering events and continuum description of the evolution of surface geometry. Using this model the evolution of an initially flat {001} surface of a thin foil of $Ni_3Al$ is studied. The calculations show the formation of a hole in the foil and the time for perforation is found to be in excellent agreement with experiment. The sputter cross section of Al atoms is found to be much higher than that of Ni atoms, indicating preferential sputtering and small concentration of Al atoms at the surface. This, together with increasing surface area due to the hole formation, explains the preferential Al loss observed experimentally.

DOI: 10.1103/PhysRevB.70.195429 PACS number(s): 68.37.Lp, 79.20.Ap, 07.05.Tp, 68.55.−a

## I. INTRODUCTION

Scanning transmission electron microscopes fitted with field emission guns (FEG STEMs) are used to perform high spatial resolution chemical microanalysis of multicomponent samples, e.g., near grain boundaries of alloys. This is because in a FEG STEM the electron beam can be focused down to ~0.5 nm while still retaining sufficient current to perform x-ray analysis or electron energy loss spectroscopy to assess the material composition.

There is evidence, however, that under conditions typical for microanalysis using electron energies between 100 and 300 keV, high beam current density can alter a specimen during analysis. For example, when using the focused 100 keV high-current-density electron probe in an ultrahigh-vacuum STEM, Muller and Silcox[1] demonstrated the preferential surface sputtering of Al from intermetallic $Ni_3Al$ thin foil by using energy dispersive x-ray analysis (EDX), and Bullough[2] found the formation of nanometer size voids and holes in an Al foil. Ozkaya *et al.*[3] observed impurity-segregation-induced hole drilling at grain boundaries of an Fe-P alloy under electron irradiation, while Shang *et al.*[4] suggested that the formation of spurious segregation profiles near grain boundaries in a thin foil of $Ni_3Al$ is due to preferential sputtering of Al atoms. Very recently, Mkhoyan and Silcox[5] observed knock-on type damage with ejection of nitrogen atoms from a sample of wurtzite InN in a STEM using a 100 keV electron beam. All these reports suggest that electron beam damage may be a limiting factor for chemical microanalysis in a FEG STEM.

On the other hand, the ability to modify the composition and structure at the surface or in the bulk of a material on a nanometer scale may have relevance to applications in nanotechnology. For instance, Niwase *et al.*[6,7] fabricated self-organized nanostructures on Au, Ag, Cu, Ni, and Fe surfaces by low-temperature electron irradiation. They observed that the aligned grooves, nanoholes and hillocks appear on the electron-exit surface and, after sufficient irradiation, the grooves and holes penetrate through the foil, finally leading to the formation of nanoslits or nanoparticles. Banhart *et al.*[8] demonstrated that electron irradiation of single and multi-shell carbon nanotubes and onions can result in the formation and self-compression of spherical concentric-shell carbon onions, originating from a surface tension induced by continuous loss of atoms owing to sputtering. Recently, Galvan *et al.*[9] produced carbon nanotubes by irradiating graphite with high doses of electrons, while Ishimaru *et al.*[10] observed a crystalline-to-amorphous phase transformation in SiC and Du *et al.*[11] reported the formation of crystalline Si nanodots in $SiO_2$ films, both induced by irradiation with 200 keV electrons. These results suggest that electron beam irradiation may be applied in the fabrication of nanostructures.

In order to develop strategy for overcoming the microanalysis problem and revealing potential applications, it is important to understand the processes and mechanisms involved in preferential sputtering and hole formation under electron irradiation. It is known that high energy electron beams can cause irradiation damage in the bulk or surface by either direct "knock-on" displacement or indirectly via electronic excitations (radiolysis). In both cases the energy transfer process must impart to the lattice atom more than the "threshold" energy to create permanent displacement. Damage by radiolysis is not significant in metals or alloys under the conditions studied here and we focus on damage arising from direct "knock-on" collision between electrons and atoms.

The main input parameter into theoretical models of the mass loss due to sputtering is the atomic sputter cross section, $\sigma$, or the sputtering yield, $Y=\sigma\rho_s$, which is the number of atoms sputtered per incident electron, where $\rho_s$ is the surface density of atoms. A simple way to estimate $\sigma$ is to calculate the differential Mott cross section of electrons as a function of either electron scattering angle or nuclear recoil angle and then integrate it up to the maximum recoil angle corresponding to the sputtering threshold energy of atoms, $E_S$.

Bradley[12] calculated the atomic sputter cross sections for all naturally occurring solid elements, assuming $E_S$ to be equal to the sublimation energy. In his calculations, a constant value of $E_S$ was assumed for an element, independent

 ©2004 The American Physical Society

of nuclear recoil angle, so that the actual nuclear recoil angles were not considered. These calculations are valuable for understanding the overall behavior of sputtering of solid elements by electrons, but theoretical treatment of real experiments requires more accurate description. In particular, to reproduce experimental results on preferential sputtering and hole formation in alloy samples examined by STEM, one should account for different sputtering rates of different atomic species and include: (1) the recoil angle dependence of $E_S$, (2) actual electron trajectories to obtain distribution of nuclear recoil energies and angles at the surface, and (3) displacement of the surface owing to sputtering.

First, $E_S$ is dependent on surface orientation relative to incident electrons, atomic species, the surface sites they occupy and the recoil direction. This information can be obtained by molecular dynamics (MD), a method used by many authors.[13–15] Second, to determine the recoil energy and direction of atoms at and near the surface, the electron trajectories in a specimen should be incorporated into the modeling, and this can be done by the Monte Carlo (MC) method as documented in the monograph by Joy.[16] Third, to describe the evolution of the shape of an initially flat surface under electron irradiation, a continuum approach can be employed and for this we need to derive a differential equation describing this process.

The paper is organized as follows: In Sec. II we present the details of the model and then, in Sec. III, describe and discuss the results obtained for the case of $Ni_3Al$ foil. Conclusions are drawn in Sec. IV.

## II. SURFACE SPUTTERING MODEL

As mentioned above, the sputtering process is controlled by the atomic sputter cross section. Below in Sec. II A we present a description for an accurate calculation of the sputter cross sections employing MD data of sputtering in combination with MC simulations of electron trajectories, and then, in Sec. II B, derive the equation for sputtering-induced surface movement.

### A. Atomic sputter cross section

The atom recoil energy, $E'$, transferred by a relativistic electron with energy $E$ through elastic collision is given by[17]

$$E' = T_m \sin^2\left(\frac{\beta}{2}\right) = T_m \cos^2 \theta, \quad (1)$$

where

$$T_m = \frac{2(E+2mc^2)E}{Mc^2}, \quad (2)$$

is the maximum recoil energy, $\beta$ and $\theta$ are the electron scattering angle and atomic recoil angle, respectively, both relative to the electron trajectory before collision, $m$ and $M$ are the electron and atomic masses, respectively, and $c$ is the speed of light. The atomic sputter cross section, $\sigma$, is given by[12]

$$\sigma = 2\pi \int_{\beta_{\min}}^{\pi} d\beta \sin\beta \frac{d\sigma}{d\Omega} = \int_{E' \geq E_S} dE' P(E',E)\sigma_E, \quad (3)$$

where $d\sigma/d\Omega$ is the differential cross section for an electron to be scattered within a solid angle $\Omega$ corresponding to atomic recoil energy $E'$, $P(E',E)$ is the probability density for an atom to recoil with energy between $E'$ and $E'+\mathrm{d}E'$, $\sigma_E = \int d\Omega(d\sigma/d\Omega)$ is the total cross section of the electron with energy $E$, and $\beta_{\min}$ is the minimum electron scattering angle corresponding to the sputtering threshold, $E_S$. Obviously, $P(E',E)$ can be obtained from Eq. (3) as

$$P(E',E) = \frac{1}{\sigma_E} \frac{d\sigma}{d\Omega} \frac{d\Omega}{dE'}. \quad (4)$$

The differential and total cross sections of an electron (in $\mathrm{cm}^2/\mathrm{atom}$) are given by[16]

$$\frac{d\sigma}{d\Omega} = 5.21 \times 10^{-21} \frac{Z^2}{E^2} \left(\frac{E+mc^2}{E+2mc^2}\right)^2 \frac{1}{[\sin^2(\beta/2)+\alpha]^2}, \quad (5a)$$

$$\sigma_E = 5.21 \times 10^{-21} \frac{Z^2}{E^2} \left(\frac{E+mc^2}{E+2mc^2}\right)^2 \frac{4\pi}{\alpha(1+\alpha)}, \quad (5b)$$

where

$$\alpha = 3.43 \times 10^{-3} \frac{Z^{0.67}}{E}, \quad (6)$$

is the screening factor that accounts for the fact that the incident electron does not see all of the charge on the nucleus because of the cloud of orbiting electrons, $E$ is the electron energy in keV, and $Z$ is the atomic number. Substituting Eqs. (1), (5a), and (5b) into Eq. (4), one obtains

$$P(E',E) = \frac{\alpha(1+\alpha)T_m}{(E'+\alpha T_m)^2}. \quad (7)$$

The atomic sputter cross section $\sigma$ can easily be calculated by using Eqs. (3), (5b), and (7), if $E_S$ is a single value and independent of electron trajectories. However, the MD simulation results presented in Sec. III show that $E_S$ is a function of angle $\theta'$ between the recoil direction and surface normal vector; hence, to calculate $\sigma$ accurately, modeling of electron trajectories is required. It is necessary to decompose the recoils with $E'$ into different $\theta'$ range for each electron trajectory so as to count those recoils that contribute to sputtering with $E'(\theta') \geq E_S(\theta')$. To do this, we introduce a new function $p(\theta',E',\hat{e})$ to account for the probability density for the recoils with $E'$ to be within $\theta'$ and $\theta'+\mathrm{d}\theta'$ for an electron trajectory with a unit directional vector $\hat{e}$. As illustrated in Fig. 1, for a given $\hat{e}$, the recoils with energy $E'$ are restricted by a recoil cone with a unique recoil angle $\theta$ relative to $\hat{e}$ and all possible recoil directions are along generatrix of the cone. When the azimuthal recoil angle $\psi$ rotates around the cone, however, the recoil angle $\theta'$ relative to surface normal vector changes with $\psi$ and $p(\theta',E',\hat{e})$ can be easily determined by choosing $\psi$ from 0 to $2\pi$ with equal probability. Thus, by employing MD data of sputtering threshold

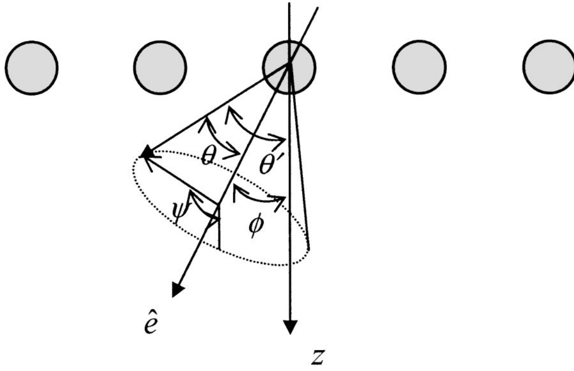


FIG. 1. A schematic diagram of atomic recoil angles relative to electron trajectory, $\theta$, and the surface normal direction, $\theta'$, respectively, the azimuthal angle $\psi$ within a recoil cone, and angle $\phi$ between the electron trajectory and surface normal direction.

energy, $E_S(\theta')$, in combination with MC simulations of electron trajectories, the atomic sputter cross section $\sigma$ can be calculated by

$$\sigma(\mathbf{r}) = \frac{2\pi}{J(\mathbf{r})}\int\int dE d\phi \sin\phi j(\mathbf{r},E,\phi) \times\left[\int\int_{E'(\theta')\geqslant E_S(\theta')} dE' d\theta' P(E',E)p(\theta',E',\hat{e})\frac{\sigma_E}{\cos\phi}\right], \quad (8)$$

where $J(\mathbf{r})=2\pi\int\int dEd\phi \sin\phi\, j(\mathbf{r},E,\phi)$ is the total flux of electrons at a unit surface area located at $\mathbf{r}$, $j(\mathbf{r},E,\phi)$ is the flux density of electrons with energy between $E$ and $E+dE$ and the angle between $\hat{e}$ and surface normal vector from $\phi$ to $\phi+d\phi$. When there is an angle $\phi$ between $\hat{e}$ and the surface normal, the probability of interaction between an electron and a surface atom becomes $\rho_s\sigma_E/\cos\phi$ instead of $\rho_s\sigma_E$, and this is included in Eq. (8). In Eq. (8), the term in square brackets is the atomic sputter cross section for a given electron trajectory with values $(E,\hat{e})$ and the integration before the brackets indicates averaging over different electron trajectories.

The atomic sputter cross section $\sigma$ defined at the specific surface position by Eq. (8) is dependent on the surface geometry. For a geometry of the electron-exit surface formed by sputtering as shown in Fig. 2, the surface outward normal direction $\mathbf{n}$ at any particular point defined by the cylindrical coordinate system $(z,\rho,\varphi)$ is given by

$$\mathbf{n} = \frac{1}{\sqrt{1+\left(\frac{\partial z}{\partial \rho}\right)^2}}\left(-\frac{\partial z}{\partial \rho}\cos\varphi\mathbf{i} - \frac{\partial z}{\partial \rho}\sin\varphi\mathbf{j} + \mathbf{k}\right), \quad (9)$$

where $\mathbf{i}$, $\mathbf{j}$, and $\mathbf{k}$ are the unit vectors of a fixed Cartesian coordinate system used in the single scattering MC model.[16] For a collision occurring at the point $(z,\rho,\varphi)$ of the surface, the recoil is directed into space rather than the specimen interior if the angle between the recoil and surface normal is less than $\pi/2$, implying that the sputter cross section in Eq. (8) depends on the surface slope. This has to be taken into consideration when calculating the sputter cross section.

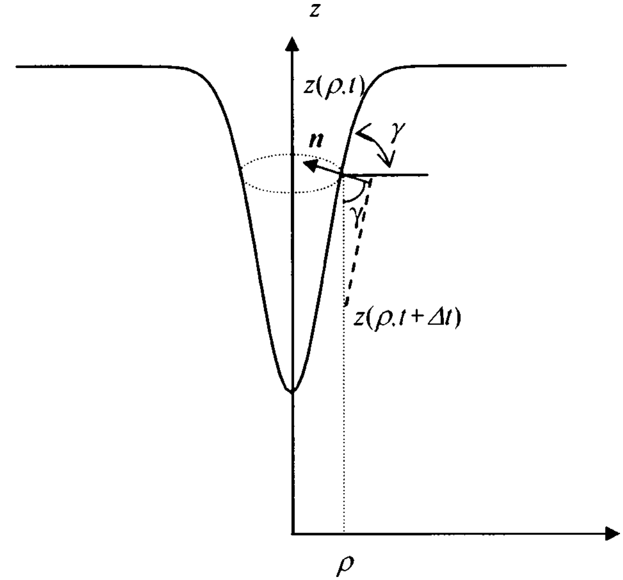


FIG. 2. A schematic diagram showing the $z$-$\rho$ cross section of the electron-exit surface formed by sputtering.

In an alloy, the different atomic species have different sputter cross sections. In the MC simulation electron trajectories were determined by elastic scattering with average cross section $\sigma_E$, given by Eq. (5b) using an average atomic number, i.e., $\bar{Z}=\frac{3}{4}Z_A+\frac{1}{4}Z_B$ for an $A_3B$ alloy or compound.[16] However, $E_S(\theta')$, $P(E',E)$, and $p(\theta',E',\hat{e})$ were specific to the atomic species in the calculation of sputter cross sections. In this way, the probability of interaction between an electron and surface atoms in an alloy is the same as in the MC code.

The cross section defined in Eq. (8) accounts for sputtering of surface atoms by direct knock-on collisions. It neglects the subsurface recoils, which are important only when the electron energy is high enough, such as 600 keV for gold foils.[18] In a FEG STEM the electron energies are typically ~200 keV and thus sputtering by subsurface recoils is insignificant.

### B. Sputtering-induced surface movement

In order to exploit the rotational symmetry around the $z$-axis of the Gaussian-type intensity profile of the stationary focused electron probe in a STEM,[2] we use a cylindrical coordinate system $(\rho,\varphi,z)$ with the origin placed in the beam center at the electron-entrance surface, and use two dimensional function $z(\rho,t)$ to describe the surface position, as illustrated in Fig. 2.

Now we derive a differential equation for the surface movement due to sputtering. Consider a binary $AB$ alloy. At the beginning of irradiation, the surface composition changes due to the difference in sputter cross sections of different atoms. The change of surface concentrations $C_A$ and $C_B$ with time can be expressed by the following continuity equations:

$$\frac{\partial C_A(\rho)}{\partial t} = -f_A(\rho)C_A(\rho) + v(\rho)\nabla C_A, \quad (10a)$$

$$\frac{\partial C_B(\rho)}{\partial t} = -f_B(\rho)C_B(\rho) + v(\rho)\nabla C_B, \quad (10b)$$

where

$$f_A(\rho) = J(\rho)\sigma_A(\rho), \quad (11)$$

is the partial sputtering frequency, which equals the reciprocal mean time required to sputter all $A$-type atoms from the surface located at $\rho$, and $v(\rho)$ is the speed of surface motion along the surface normal direction. In Eqs. (10a) and (10b), the first term on the right-hand side represents the decrease in number of atoms due to sputtering, while the second term accounts for the increase in number of atoms of the same type arising from emergence of new surface due to surface movement. The atomic concentration gradient can be approximated as $\nabla C_A = C_A^0/h$, where $C_A^0$ is the concentration of $A$-type atoms in the bulk of the specimen and $h$ is the thickness of the monatomic surface layer.

An assumption is made that after a time, the surface composition reaches dynamic equilibrium and does not change with time. In this case, using detailed balance approximation [i.e., taking $(\partial C_A/\partial t) = (\partial C_B/\partial t) = 0$] we obtain the speed of surface motion in the direction of the surface normal equal to

$$v(\rho) = h\frac{f_A(\rho)f_B(\rho)}{f_A(\rho)C_B^0 + f_B(\rho)C_A^0}, \quad (12)$$

and the quasiequilibrium surface concentration $C_A(C_A + C_B = 1)$ is

$$C_A(\rho) = \frac{f_B(\rho)C_A^0}{f_A(\rho)C_B^0 + f_B(\rho)C_A^0}. \quad (13)$$

The equation for the surface motion can be deduced using simple geometry consideration shown in Fig. 2, and is

$$\frac{\partial z(\rho,t)}{\partial t} = -v(\rho)/\cos\gamma = -v(\rho)\sqrt{1 + \left(\frac{\partial z(\rho,t)}{\partial \rho}\right)^2}, \quad (14)$$

where $\tan\gamma = (\partial z(\rho,t)/\partial\rho)$ represents the tangent slope of the surface curve at time $t$.

The number of bonds and stoichiometry for the surface atoms change in the course of sputtering, resulting in change of binding energy and sputter cross section of atoms. To account for this, we choose an average sputter cross section as the mean of the sputter cross section of an atom in the surface and that of an adatom on the surface. For instance, for a $Ni_3Al$ (001) surface we take the average sputter cross section of Ni atoms in the alternating Ni-Al mixed (denoted as "M") and pure Ni (denoted as "N") layers as

$$\bar{\sigma}_{Ni}(\rho) = \frac{2\sigma_1(\rho)\sigma_2(\rho)}{\sigma_1(\rho) + \sigma_2(\rho)}, \quad (15)$$

where $\sigma_1$ and $\sigma_2$ are sputter cross sections of Ni in or on the N layer, respectively. This is because the sputtering frequency of Ni atoms in an M layer is actually determined by the cross section of the Ni adatom due to fast sputtering of Al atoms (see Fig. 5 below), converting the remaining Ni atoms into adatoms on the N layer below. This average sputter cross section of Ni atoms in Eq. (15) is then applied in Eqs. (11), (12), and (14) to obtain the average speed of surface movement along the [001] direction.

Now the framework of the model is established. To model surface evolution under electron irradiation, we divide the specimen into a series of concentric cylinders that intersect the surface in circular annuli described by $\rho_i$. We use MC simulation of electron trajectories to determine the sputter cross sections in all these surface sections and the time step needed to sputter one atomic layer in the center zone, and then change the surface according to Eqs. (12) and (14). At each step the surface slope is determined as $[z(\rho_{i+1}) - z(\rho_i)]/(\rho_{i+1} - \rho_i)$ for each $i$, and is used in Eqs. (8) and (9) to calculate the sputter cross sections at $\rho_i$. The above process is then repeated to simulate the surface evolution with time.

To understand the preferential sputtering in a binary alloy during irradiation, we need to calculate the number of sputtered $A$- and $B$-type atoms, $N_A$ and $N_B$, or their ratio $N_A/N_B$. The number of $A$-type atoms at the electron-exit surface is given by integration over this surface:

$$n_A = \int_S C_A(\rho)\rho_s ds. \quad (16)$$

It is readily shown that the numbers of sputtered $A$ and $B$ atoms, $N_A$ and $N_B$, obey the relationship

$$\frac{n_A + N_A}{n_B + N_B} = \frac{C_A^0}{C_B^0}. \quad (17)$$

Hence, the number of $A$ atoms sputtered by the time $t$ is equal to

$$N_A(t) = C_A^0[N(t) + n_B] - C_B^0 n_A, \quad (18)$$

where $N(t)$ is the total sputtered atoms at time $t$, equal to sputtered volume divided by the average atomic volume. Exchange of subscripts $A$ and $B$ in this equation provides equation for $N_B(t)$. The sputtering rate $S(t)$ and sputtering yield $Y(t)$ averaged over the time $t$ can be obtained by

$$S(t) = N(t)/t, \quad (19)$$

$$Y(t) = S(t)/I, \quad (20)$$

where $I$ is the electron current (i.e., number of electrons emitted per second).

It should be pointed out that Eq. (10) neglects processes such as irradiation-enhanced diffusion,[19,20] and redeposition of atoms sputtered from another surface area. To model electron-stimulated diffusion along a side wall of a hole formed at the electron-exit surface by sputtering would be a challenging task, and to account for redeposition it would be necessary to consider the sputtered atom trajectory, which is influenced by the neighbors of the sputtered atom at or near the surface (see MD study by Cherns *et al.*[18]). These features would complicate the modeling very significantly. Though their neglect excludes some detail of surface evolution, such as void formation by sealing of the hole, the results obtained

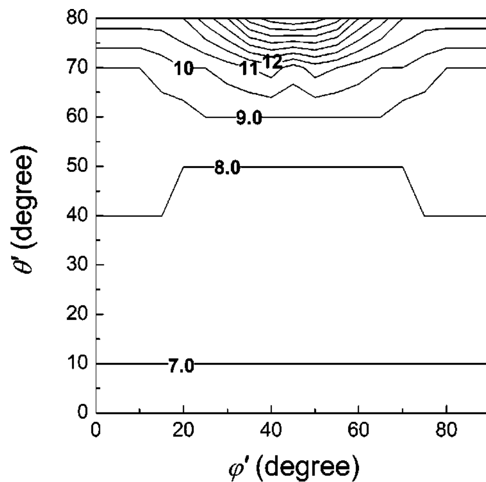


FIG. 3. The energy contour (in eV) for sputtering of Al atoms in the (001) M-layer surface of $Ni_3Al$. The atomic recoil direction is indicated by $(\theta', \varphi')$, where $\theta'$ is the angle between recoil direction and surface normal direction ($z$-axis) and $\varphi'$ is the angle between the perpendicular projection of recoil direction on the (001) plane and the [100] direction ($x$-axis).

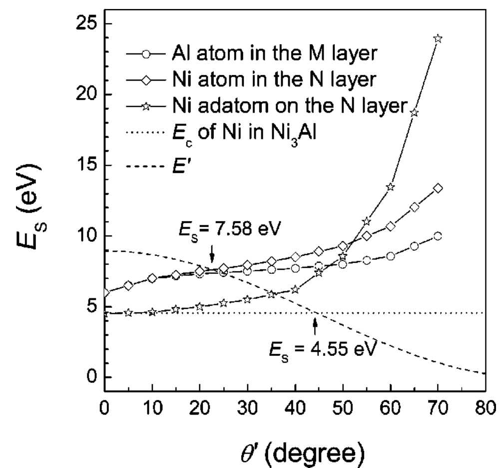


FIG. 4. Sputtering threshold energy as a function of $\theta'$ obtained by MD simulations for Al, Ni atoms and Ni adatom. The sublimation energy $E_c$ of Ni in the $Ni_3Al$ and the recoil energy $E'$ of Ni atoms transferred by 200 keV electrons are shown by dotted and dashed lines, respectively. The minimum $E_S$ that can result in a sputter of atoms by electrons is determined by the crossover points between the atomic recoil energy and the sputtering threshold energy.

by the present model compare well with experiment and are valuable for understanding hole formation and preferential sputtering.

## III. RESULTS AND DISCUSSIONS

The model is applied to study the evolution of the initially flat {001} surface of the ordered $Ll_2$ alloy $Ni_3Al$. We have studied sputtering events at and near this surface in detail by MD and the results are summarized in Sec. III A. Our predictions for surface evolution are presented in Sec. III B and compared with those of colleagues at the University of Birmingham who have conducted experiments on this system.[21]

### A. MD results of sputtering threshold energy

The many-body potential of $Ni_3Al$ derived by Vitek *et al.*[22] and modified for short range interaction by Gao and Bacon[23] was employed in this study. This potential has been used to determine displacement thresholds in the bulk of $Ni_3Al$ (Ref. 23) and the results were confirmed by experiments.[24] Figure 3 presents the energy contours calculated for sputtering of Al atoms in the (001) M layer surface of a $Ni_3Al$ foil for different recoil directions. As can be seen, $E_S$ is almost independent of the azimuthal angle $\varphi'$ when $\theta' < 70°$. Thus, it can be expressed as a function of $\theta'$ as shown in Fig. 4, which is obtained by averaging the energy over $\varphi'$. $E_s$ for a Ni atom in the N layer and a Ni adatom on the N layer are also shown in Fig. 4: the trend is for $E_S$ to increase with increasing $\theta'$, particularly at large $\theta'$. Interestingly, $E_S$ for the Ni adatom is lower than that of a Ni atom in the N layer when $\theta' < 53°$ but higher when $\theta' > 53°$. This is because a Ni adatom has less bonds with the other atoms than an atom in the surface, which makes it easier to be sputtered at small $\theta'$, whereas at high $\theta'$, it glances off the surface and drags underlying atoms, thus requiring more energy to escape from the surface.

It is seen from Fig. 4 that the smallest $E_S$ occurs for recoils along the surface normal direction (at $\theta'=0$) and is 6.0 eV for both Al and Ni atoms in the (001) surface layer, which is larger than the sublimation energy of 4.63 (Al) and 4.55 (Ni) eV in $Ni_3Al$. The smallest $E_S$ for a Ni adatom on the N layer surface is 4.5 eV, which is close to the Ni sublimation energy but larger than the binding energy of 3.57 eV for the Ni adatom on the N layer surface. Obviously, the sputter cross-sections determined by $E_S$ obtained from MD results will be different from those determined by the sublimation energy. To see this difference, we take Ni atoms as an example and assume for simplicity that all electrons pass through the electron-exit surface along the surface normal direction so that the recoil energy in Eq. (1) is a simple function of $\theta'$ owing to $\theta' = \theta$. The recoil energy transferred by 200 keV electrons as a function of $\theta'$ is shown in Fig. 4. The minimum $E_S$ that can result in sputter of atoms by electrons can be determined by the crossover points between the atomic recoil energy and the sputtering threshold energy. They are 7.58 and 5.85 eV for Ni atom in and Ni adatom on the N layer surface, respectively, compared with the sublimation energy of 4.55 eV for Ni atoms in $Ni_3Al$. The corresponding sputter cross sections $\sigma$ calculated by Eq. (3) using Bradley's code[12] are 49.08, 163.34, and 328.75 barns. The average $\bar{\sigma}$ for Ni atoms at the (001) surface can be calculated by Eq. (15) and it is 75.48 barn, i.e., less than one-quarter of the value obtained with the sublimation energy. It is therefore concluded that the dependence of $E_S$ on recoil direction has a significant influence on the atomic sputter cross sections.

### B. Surface sputtering and evolution

The sputter cross sections calculated accurately by Eq. (8) are found to be independent of $\rho$ in an initially-flat surface,

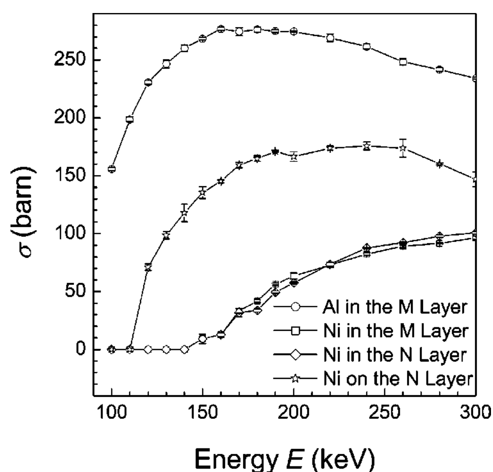


FIG. 5. Sputter cross sections versus the electron energy for Al and Ni atoms at the (001) surface of a $Ni_3Al$ foil of 62.5 nm thickness. Ni on the N layer stands for a Ni adatom on the N layer surface. 1 barn$=10^{-24}$ cm$^2$.

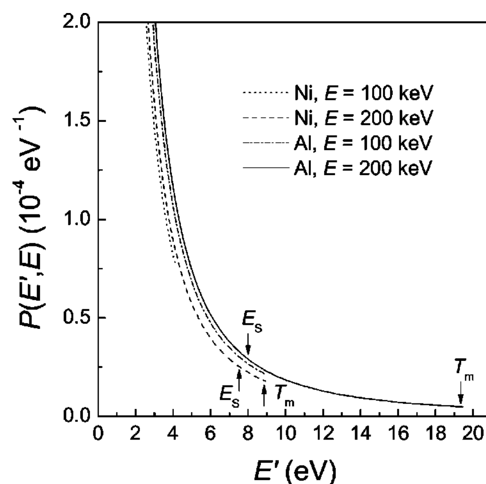


FIG. 6. The recoil probability density $P(E',E)$ as a function of recoil energy $E'$ transferred by electrons with energy $E$. Each curve is drawn up to maximum recoil energy, $T_m$, at right end, as indicated by arrows for the case of $E=200$ keV. The minimum sputtering threshold, $E_S$, determined by the way shown in Fig. 4 is also indicated by arrows for the case of $E=200$ keV.

despite the existence of a profile of electron current density and broadening of the beam at the electron-exit surface. Figure 5 shows the sputter cross sections of Al and Ni atoms at this surface for a $Ni_3Al$ specimen of 62.5 nm thickness. The sputter cross sections of Al atoms and Ni adatoms first increase with increasing electron energy, then reach a maximum before decreasing, whereas those of Ni atoms in the M or N layers increase monotonously after the electron energy exceeds a threshold value of 141 keV. A prominent feature of the figure is that the sputter cross section of an Al atom is higher than that of a Ni adatom, and much higher than that of a Ni atom in the surface with either M or N layer outermost. This is the main reason for the preferential sputtering of Al atoms observed in experiments.

To understand the change of the sputter cross sections with increasing electron energy, let us look back at Eq. (3). The atomic sputter cross section, $\sigma$, is proportional to the total scatter cross section of electrons, $\sigma_E$, namely $\sigma=k\sigma_E$, with a sputter coefficient $k=\int_{E_S}^{T_m}dE'P(E',E)$. Figure 6 gives the recoil probability density $P(E',E)$ as a function of recoil energy $E'$, together with the indication of the minimum $E_S$ determined by the way shown in Fig. 4 for the case of 200 keV electrons. For a case of 100 keV electrons, because the maximum recoil energy $T_m$ of 4.1 eV for Ni is less than minimum $E_S$ of 4.5 eV for a Ni adatom on an N layer, the sputter cross section of Ni is zero, indicating that $k=0$ if $T_m<E_S$. The sputter coefficient $k$ increases with increasing electron energy, because both $P(E',E)$ and $T_m$ increase with increasing electron energy $E$, as seen in Fig. 6 that the curve for $E=200$ keV is above that for $E=100$ keV. The total scatter cross section of electrons, $\sigma_E$, however, decreases with increasing electron energy owing to the Coulomb nature of the cross section in Eq. (5b). As a result, the change of the atomic sputter cross sections with increasing electron energy is determined by the competition between $k$ and $\sigma_E$. Thus, the initial increase of sputter cross section of Al atoms and Ni adatoms in Fig. 5 is due to influence of $k$, while the decrease is because $k$ loses influence owing to the rapid decrease of $P(E',E)$ at high $E'$. As can be seen from Fig. 6, $P(E',E)$ that contributes to sputtering is around the magnitude of $10^{-5}$ eV$^{-1}$ and the magnitude of the maximum recoil energy $T_m$ transferred by several hundred keV electrons is about 1–10 eV, suggesting that the sputter coefficient $k$ has a magnitude of $10^{-5}$–$10^{-4}$.

Figure 6 can also explain why Al is sputtered more efficiently than Ni. The sputter coefficient $k$ can be obtained by integrating from $E_S$ to $T_m$, i.e., from the area underneath the curve between $E_S$ and $T_m$. It is seen that at the same electron energy, e.g., 200 keV, this area for Al is much larger than that for Ni, indicating that the sputter coefficient $k$ of Al is much larger. This arises because both $P(E',E)$ and $T_m$ are larger for Al than Ni due to the mass and atomic number difference. The maximum recoil energy of Al is about twice that of Ni because the mass of Al is approximately half that of Ni [see Eq. (2)]. This is the main contribution to the difference in the sputter coefficient $k$.

The calculated evolution of the electron-exit surface of a $Ni_3Al$ specimen with thickness 62.5 nm under electron irradiation is shown in Fig. 7. The Gaussian-type shape of the electron-exit surface formed by sputtering is due to the profile of the incident electron probe. Figure 8 gives the time evolution of the film thickness at the cylinder center $\rho=0$ and the ratio of the number of sputtered Al to sputtered Ni atoms. As can be seen from the figure, the perforation of the foil due to sputtering is predicted to take 58 s. Because the atomic recoil angle $\theta$ and the electron scattering angle $\beta$ obey the relationship $2\theta+\beta=\pi$, $\theta\leqslant\pi/2$ implies that there is no redeposition of sputtered atoms at the spot $\rho=0$ corresponding to the center of the electron beam. Thus, the output of the model in this region can be compared directly with experiment. The change of thickness of this region with time can be measured in a STEM and, although it is difficult to determine experimentally the detailed shape change due to fast sputtering, the time when a hole through a sample is first

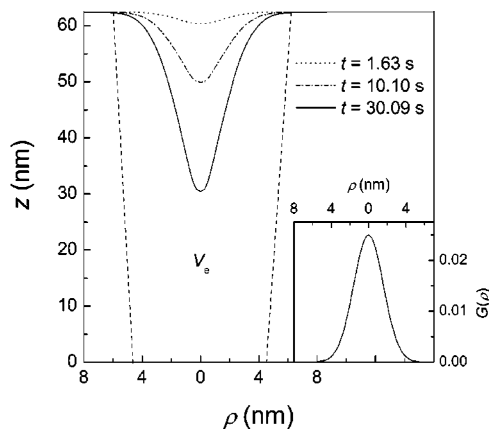


FIG. 7. Evolution of the shape of electron-exit surface of a $Ni_3Al$ specimen of 62.5 nm thickness irradiated by 200 keV electrons with the beam Gaussian standard deviation $\delta=1.6$ nm and current 2.23 nA. The electron probe is incident on the lower surface at $z=0$ and its initial profile $G(\rho)=(1/\sqrt{2\pi}\delta)e^{(\rho^2/2\delta^2)}$ is shown in the inset. Two dashed lines are schematically drawn to show a region of the effective volume, $V_e$, detected by the electron probe. The size of this region at the electron-entrance surface is the same as the electron beam size while that at the electron-exit surface is broadened due to scatter of electrons in the film.

formed can be estimated. For the same conditions as used in Fig. 6, the time for the hole formation determined in experiment is about 60 s,[21] in excellent agreement with our result of ~58 s.

As can be seen from Fig. 8, the ratio of sputtered Al to sputtered Ni atoms decreases with time rapidly up to ~5 s and then more slowly. The preferential sputtering of Al atoms is evident from the fact that this ratio is higher than the bulk Al atomic fraction of 0.25 (dashed line in Fig. 8). In the experiment, the measured ratio of the number of Ni to Al atoms in the specimen increases with time,[21] implying preferential loss of Al atoms, consistent with our results. Figure 7 shows schematically the effective volume, $V_e$, within the two long dashed lines, from which the composition of the foil is measured by the electron probe. The ratio of Ni to Al determined in experiment can be expressed as

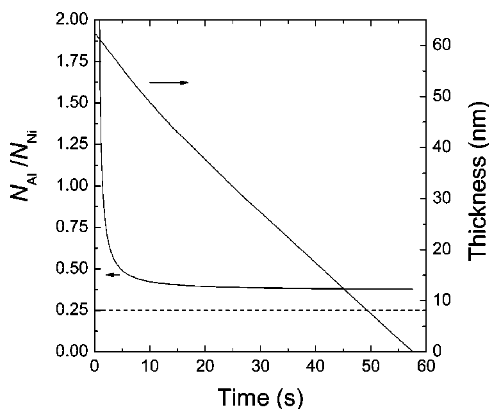


FIG. 8. Variation of the film thickness in the beam center and the ratio of sputtered Al to Ni atoms with time. The dashed line shows the bulk Al composition in a $Ni_3Al$ specimen.

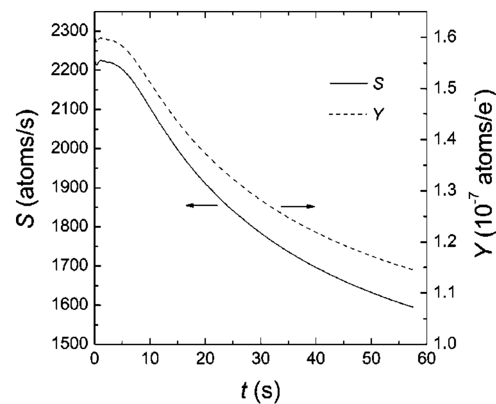


FIG. 9. Variation of sputtering rate and sputtering yield with time.

$$\frac{C^0_{\mathrm{Ni}}[V_e - V(t) - V_s] + n_{\mathrm{Ni}}}{C^0_{\mathrm{Al}}[V_e - V(t) - V_s] + n_{\mathrm{Al}}} \approx \frac{C^0_{\mathrm{Ni}}}{C^0_{\mathrm{Al}}} + \frac{\rho_s A_s}{C^0_{\mathrm{Al}}[V_e - V(t) - V_s]}, \tag{21}$$

where $V(t)$ and $V_s$ are the volumes of sputtered region and surface layer, respectively, $n_{\mathrm{Ni}}$ and $n_{\mathrm{Al}}$ are the numbers of Ni and Al atoms at the electron-exit surface, respectively, and $A_s$ is the surface area. To obtain the right-hand side of Eq. (21), we used Eq. (16) and assumed that $C_{\mathrm{Al}}$ $(n_{\mathrm{Al}})$ is equal to zero due to the much larger sputter cross section of Al (see Fig. 5). Equation (21) indicates that the increase of the ratio of the number of Ni to Al atoms observed in experiment arises from the second term on the right side, where the numerator increases due to increased surface area $A_s$ and the denominator decreases due to sputtering. We therefore conclude that the preferential loss of Al atoms originates from a much higher sputter cross section of Al than Ni atoms, together with the increase of the area of electron-exit surface due to the hole formation during irradiation.

Figure 9 gives the variation of sputtering rate and sputtering yield with time. During the first few seconds the sputtering rate and yield remain almost constant and after that start to decrease. This decrease is due to formation of the Gaussian-type hole shown in Fig. 7, which results in smaller sputter cross sections at the side wall of the hole than at the initial planar surface. As already mentioned in Sec. II, the present model neglects the redeposition process of sputtered atoms and, hence, gives the upper limits for the sputtering rate and yield. The sputtering rate determined in the experiment was 620 atoms/s at $t=70$ s when a hole was formed with 2 nm diameter in the electron-entrance surface and 4 nm diameter in the electron-exit surface.[21] This value is about half the present theoretical estimate, for the reason already described above.

## IV. CONCLUSIONS

A new multiscale model for the description of the surface sputtering and evolution under electron irradiation in a STEM has been proposed. It employs MD results of sputtering threshold energies and the MC simulation of electron trajectories to determine the sputter cross section of atoms at

the electron-exit surface. A continuum differential equation describing the surface evolution due to sputtering has been derived.

Application of the model to a $Ni_3Al$ thin foil with the {001} surface has revealed hole formation and preferential sputtering of Al atoms consistent with experiment. The predicted rate of the hole formation is in good agreement with experiment.

The sputter cross section of Al atoms has been found to be much higher than that of Ni atoms, resulting in a reduced concentration of Al at the surface. This and the increase of surface area due to hole formation are the two major reasons for the preferential Al loss observed.

Further development of the model for treating sputtering phenomena in a FEG STEM would require inclusion of void formation due to sealing of the hole that first forms at the electron-exit surface. In particular it would be necessary to take into consideration the redeposition process of sputtered atoms as well as the irradiation-enhanced diffusion.

## ACKNOWLEDGMENTS

The authors would like to thank Professor D.C. Joy of the University of Tennessee at Knoxville for providing the Monte Carlo code to calculate electron trajectories and Dr. T.J. Bullough of the University of Liverpool for stimulating discussions. Thanks are also due to Professor I.P. Jones and Mr. B.B. Tang of the University of Birmingham for valuable discussions of their experimental results and the model proposed here during the course of collaborative work. The authors acknowledge the Engineering and Physical Sciences Research Council for provision of financial support.

*Author to whom correspondence should be addressed. Email address: wslai@tsinghua.edu.cn; presently at Advanced Materials Laboratory, Department of Materials Science and Engineering, Tsinghua University, Beijing 100084, China.

[1] D. A. Muller and J. Silcox, Philos. Mag. A **71**, 1375 (1995).
[2] T. J. Bullough, Philos. Mag. A **75**, 69 (1997).
[3] D. Ozkaya, J. Yuan, L. M. Brown, and P. E. J. Flewitt, J. Microsc. **180**, 300 (1995).
[4] P. Shang, R. Keyse, I. P. Jones, and R. E. Smallman, Philos. Mag. A **79**, 2539 (1999).
[5] K. A. Mkhoyan and J. Silcox, Appl. Phys. Lett. **82**, 859 (2003).
[6] K. Niwase, F. Phillipp, and A. Seeger, J. Appl. Phys. **39**, 4624 (2000).
[7] K. Niwase and H. Abe, Mater. Trans., JIM **43**, 646 (2002).
[8] F. Banhart, T. Fuller, P. Redlich, and P. M. Ajayan, Chem. Phys. Lett. **269**, 349 (1997).
[9] D. H. Galvan, R. Rangel, and E. Adem, Fuller. Nanotub. Car. N. **11**, 285 (2003).
[10] M. Ishimaru, I. T. Bae, and Y. Hirotsu, Phys. Rev. B **68**, 144102 (2003).
[11] X. W. Du, M. Takeguchi, M. Tanaka, and K. Furuya, Appl. Phys. Lett. **82**, 1108 (2003).
[12] C. R. Bradley, Argonne National Laboratory Report No. ANL-88-48 (1988).
[13] D. P. Jackson, Can. J. Phys. **53**, 1513 (1975).
[14] P. Sigmund *et al.*, Nucl. Instrum. Methods Phys. Res. B **36**, 110 (1989).
[15] H. Gades and H. M. Urbassek, Nucl. Instrum. Methods Phys. Res. B **69**, 232 (1992); **88**, 218 (1994).
[16] D. C. Joy, *Monte Carlo Modelling for Electron Microscopy and Microanalysis* (Oxford University Press, Oxford, 1995), Chap. 3.
[17] F. Seitz and J. S. Koehler, Solid State Phys. **2**, 307 (1956).
[18] D. Cherns, M. W. Finnis, and M. D. Matthews, Philos. Mag. **35**, 693 (1977).
[19] S. Ohta and H. Takahashi, J. Electron Microsc. **48**, 899 (1999).
[20] Y. Mera, K. Suzuki, and K. Maeda, Physica B **340**, 488 (2003).
[21] B. B. Tang, I. P. Jones, W. S. Lai, and D. J. Bacon (unpublished).
[22] V. Vitek, G. J. Ackland, and J. Cserti, Mater. Res. Soc. Symp. Proc. **186**, 227 (1990).
[23] F. Gao and D. J. Bacon, Philos. Mag. A **67**, 275 (1993).
[24] C. Dimitrov, B. Sitaud, and O. Dimitrov, J. Nucl. Mater. **208**, 53 (1994).